Journal of Ultrafine Grained and Nanostructured Materials
https://jufgnsm.ut.ac.ir
Vol. 59, No.1, June 2026, pp. 116-125
Print ISSN: 2423-6845 Online ISSN: 2423-6837
DOI: 10.22059/jufgnsm.2026.01.09

PEO–Hydrothermal Engineering of VO_x/TiO_2 Photocatalysts for Efficient Visible-Light Degradation of Methylene Blue

Shiva Zaheri[1], Arash Fattah-alhosseini[1,*], Minoo Karbasi[1], Mosab Kaseem[2,*]

[1]Bu-Ali Sina University, Department of Materials Engineering, Faculty of Engineering, Hamedan, Iran
[2]Sejong University, Department of Nanotechnology and Advanced Materials Engineering, Seoul 05006, Republic of Korea

Recieved: 24 November 2025 ; Accepted: 3 May 2026

[*]Corresponding author, E-mail: a.fattah@basu.ac.ir , mosabkaseem@sejong.ac.kr

ABSTRACT

Visible-light-driven photocatalysis plays a crucial role in sustainable wastewater treatment. In this work, Methylene blue (MB) was employed as a model organic pollutant to evaluate the photocatalytic performance of VO_x/TiO_2 composite coatings fabricated via plasma electrolytic oxidation (PEO) followed by hydrothermal treatment. The hydrothermal temperature (160–200 °C) was systematically investigated as the key operating variable. Structural and optical properties were analyzed using XRD, SEM, UV–Vis DRS, and PL spectroscopy. The optimized sample synthesized at 180 °C exhibited an apparent optical band gap of ~1.75 eV and a pronounced red-shift compared to pristine TiO_2 (~3.2 eV). Under visible-light irradiation (54 mW cm^{-2}), the 180 °C sample achieved 85% methylene blue degradation within 2.5 h, compared to only 23% for pristine TiO_2, corresponding to a 62 percentage-point improvement. Moreover, the apparent reaction rate constant increased from 2×10^{-3} to 11×10^{-3}, representing an approximately 5.5-fold enhancement. The degradation efficiency increased from 73% at 160 °C to 85% at 180 °C but decreased to 58% at 200 °C, confirming the existence of an optimal hydrothermal temperature window. The enhanced activity is attributed to improved crystallinity, extended visible-light absorption, and suppressed charge recombination at the VO_x/TiO_2 interface. These findings highlight the importance of hydrothermal temperature control in engineering efficient visible-light photocatalysts.

Keywords: *Plasma electrolytic oxidation (PEO); VO_x/TiO_2 composite; Methylene blue (MB); Photocatalytic activity; Hydrothermal.*

1. Introduction

Titanium dioxide (TiO_2)–based photocatalysts have been extensively studied due to their chemical stability, non-toxicity, and low cost, making them promising candidates for water purification and the degradation of organic contaminants [1–3]. Nevertheless, the photocatalytic activity of pristine TiO_2 is intrinsically restricted by its wide band gap and the rapid recombination of photogenerated charge carriers [4], limiting its efficiency under visible-light irradiation.

To address these challenges, surface modification or coupling TiO_2 with transition-metal oxides—particularly vanadium oxides—has emerged as an effective approach to extend visible-light absorption, suppress charge recombination, and enhance overall photocatalytic performance [5,6]. Several synthesis routes have been employed

to fabricate metal-oxide-modified TiO_2 structures, among which PEO and hydrothermal processing are particularly advantageous due to their ability to produce strongly adhered oxide coatings and well-controlled nanostructured morphologies [5,7–10].

Recent studies have emphasized that hydrothermal parameters, especially reaction temperature and duration, critically influence the morphology, crystallinity, particle size, and optical behavior of photocatalysts. For example, Jalil et al. (2022) investigated hydrothermally synthesized V_2O_5 and reported that lower temperatures (≈100 °C) resulted in narrower band gaps (≈2.08–2.15 eV), improved visible-light absorption, and consequently enhanced MB degradation [11]. On the other hand, several studies have shown that higher hydrothermal temperatures can also offer significant advantages, particularly in improving crystallinity and stabilizing the desired crystal phase.

For instance, in a study on $BiVO_4$, Truong et al. [12] demonstrated that hydrothermal synthesis at 200 °C resulted in superior crystallinity, reduced compressive strain on the dominant crystal facets, and ultimately improved photocatalytic performance in MB degradation. These observations confirm that elevated temperatures may promote the formation of more structurally optimized photocatalysts, which is critical for achieving high overall activity. Considering these contrasting principles—lower temperatures favoring band-gap narrowing and enhanced visible-light absorption, and higher temperatures promoting improved crystallinity and phase optimization—the precise control and optimization of hydrothermal temperature becomes crucial in the synthesis of VO_x/TiO_2 photocatalysts. Plasma electrolytic oxidation (PEO) is a versatile surface engineering technique capable of producing porous, ceramic-like oxide coatings with strong adhesion to metallic substrates, which can act as effective scaffolds for subsequent catalytic functionalization (e.g., incorporation or growth of active phases) [13,14]. In addition to mechanical robustness, PEO coatings provide multifunctional properties such as corrosion and wear resistance, while offering a large interfacial area beneficial for catalytic applications [13]. However, the discharge-driven nature of the PEO process often leads to the formation of micropores and microcracks, which may result in structural non-uniformity, and relatively high energy consumption can be considered a practical limitation of this technique [14,15]. Hydrothermal treatment, as a post-modification approach, enables controlled nucleation and crystal growth and is widely used to tailor crystallinity and surface chemistry under relatively mild conditions [16,17]. Nevertheless, hydrothermal synthesis typically requires pressurized autoclaves, strict temperature control, and relatively long reaction times, which may affect reproducibility and scalability if not carefully optimized [16].

Therefore, the combination of PEO and hydrothermal treatment offers a balanced strategy by integrating the advantages of both methods while mitigating their individual limitations, enabling the fabrication of uniform VO_x/TiO_2 heterostructures with improved crystallinity, controlled loading, and enhanced photocatalytic performance [17,5]. In this study, while maintaining a fixed precursor concentration (6 mM) and reaction time (24 h) selected from preliminary screening experiments, the hydrothermal temperature (160–200 °C) was systematically investigated to determine the optimal conditions for photocatalytic MB degradation. Despite the advancements in hydrothermal modification strategies, there remains a lack of comprehensive optimization studies focusing on VO_x-modified TiO_2 layers synthesized via the PEO method. In particular, the interplay between vanadium concentration, hydrothermal temperature, and reaction duration—and their collective influence on photocatalytic activity—has not been fully elucidated.

In this work, TiO_2 layers were first fabricated via PEO, followed by hydrothermal deposition of vanadium oxide. Through systematic evaluation of hydrothermal temperature (160–200 °C), while maintaining a fixed vanadium precursor concentration (6 mM) and reaction time (24 h) selected from preliminary screening, the optimized VO_x/TiO_2 coating achieved 85% MB degradation within 2.5 h under visible-light irradiation. Notably, although ~180 °C is commonly adopted as a standard hydrothermal condition in related studies, both lower and higher temperatures were intentionally examined in this work to identify the optimal temperature window for VO_x growth on PEO–TiO_2 coatings.

This study highlights the effectiveness of the combined PEO–hydrothermal modification strategy and underscores the critical role of hydrothermal temperature in tailoring the photocatalytic performance of VO_x/TiO_2 for environmental applications.

2. Materials and Methods

2.1. Chemical substances and reagents

Grade 2 pure titanium plates ($2 \times 1.5 \times 0.1$ cm^3) were used as substrates. $Na_3PO_4 \cdot 12H_2O$, KOH, NaCl, vanadium oxide, and 33% H_2O_2 were obtained from Merck Co. All synthesis steps and treatments were carried out in deionized (DI) water, and all scavengers, including Isopropanol (C_3H_8O), Sodium azide (NaN_3), and Benzoquinone ($C_6H_4O_2$) were obtained from Sigma Aldrich Co.

2.2. Synthesis of PEO coatings and subsequent hydrothermal modification

Prior to the PEO treatment, commercially pure titanium substrates were mechanically polished using SiC abrasive papers (up to 1200 grit), ultrasonically cleaned in acetone and ethanol for 10 min each, rinsed with deionized water, and dried in air. A pulsed DC power supply (PM700/7 PRC) was employed to generate the PEO coatings in a phosphate-based electrolyte. The principal operating conditions influencing the coating process were earlier documented by Saberyoun et al [18]. In the present work, the coating produced under these conditions is designated as sample T, and the detailed processing parameters are summarized in the left column of Table 1.

For hydrothermal deposition of vanadium oxide onto TiO_2, a 6 mM precursor solution was obtained by dissolving the appropriate amount of vanadium oxide in a 48 mL solvent mixture containing 45 mL DI water and 3 mL H_2O_2, resulting in a transparent brown solution. After stirring for 30 minutes, the solution was placed into a 50 mL stainless-steel autoclave lined with Teflon. The pH was adjusted to 2, and the reactor was maintained at the selected hydrothermal temperature (160, 180, 200 °C) for 24 hours. TiO_2 coatings were mounted on a supporting holder inside the autoclave to guarantee direct contact with the reaction medium. A schematic representation of the synthesis process is shown in Figure 1.

Table 1- Designations of samples and the experimental conditions employed in the PEO and subsequent hydrothermal treatments

	ID	PEO conditions		ID	Vanadium oxide (mM)	Time (h)	Temperature (°C)
PEO process	T	$Na_3PO_4.5H_2$ (5 g/L) KOH (4 g/L) f = 1000 Hz, D = 80 % I = 12A/dm^2, t = 10 min	Hydrothermal	TV-160	6	24	160
				TV-180			180
				TV-200			200

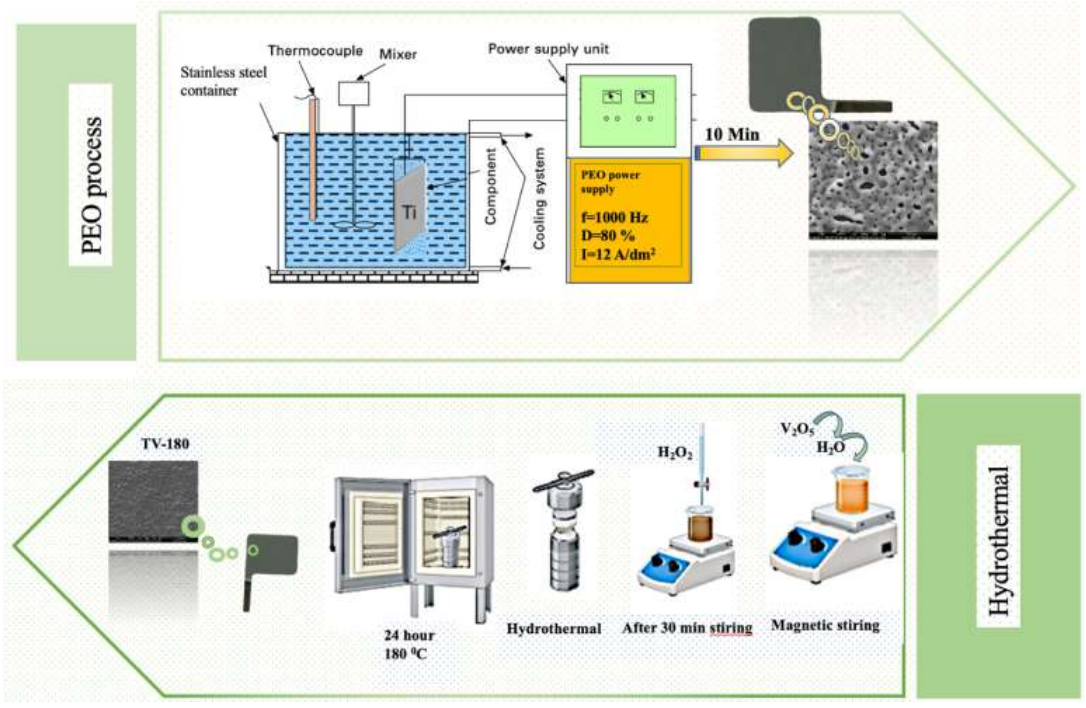

Fig. 1- Schematic representation of PEO layer formation followed by hydrothermal processing.

2.3. Characterizations

Surface morphology was analyzed using SEM (JEOL JSM-840A), while further microstructural characteristics were investigated through FE-SEM equipped with an EDS detector (Silicon Drift 2017). XRD analysis was carried out on a PHILIPS PW1730 diffractometer employing CuKα radiation (λ = 1.5406 Å) at room temperature, with diffraction patterns recorded over the 2θ range of 20–80° at a step size of 0.05°. Surface wettability was measured with a goniometer using 1 µL DI water droplets, and the average values were obtained from three readings for each layer. UV–Vis DRS (Shimadzu) was employed to examine the spectral reflectance properties of the coatings and to determine their band-gap energies. The photoluminescence (PL) response of the best-performing layer was captured using a spectrofluorometer (Perkin Elmer Lambda 25) with a Cd-He laser excitation source at 325 nm.

2.4. Evaluation of photocatalytic properties of coatings

The photocatalytic activity of the PEO coatings was evaluated through the degradation of MB. Coating samples with an active area of 6 cm^2 were immersed in 30 mL of a 10 ppm MB solution and exposed to a 100 W visible LED light source positioned 10 cm above the sample surface. The irradiance at the sample surface was measured using a radiometer and found to be 54 mW cm^{-2}. Before light exposure, the suspension was agitated in the dark for 30 minutes to achieve adsorption–desorption equilibrium.

$$Photodegradation\ rate = \frac{C_0 - C_t}{C_0} \times 100 \qquad (1)$$

The progress of the photocatalytic reaction was monitored by measuring the decrease in absorbance using a UV–Vis spectrophotometer (Agilent Cary 60). The photocatalytic degradation efficiency (%) was calculated according to Eq. (1), where C_0 and C_t correspond to the MB concentrations after dark adsorption equilibrium (before illumination) and after irradiation for time t, respectively.

3. Results and Discussion

The hydrothermal temperature was found to strongly influence the structural and photocatalytic behavior of VO_x/TiO_2 composite coatings. As shown in Figure 2, samples treated at 180 °C exhibited the highest photocatalytic activity toward MB degradation, achieving 85% MB removal within 2.5 h. In contrast, coatings prepared at 160 °C displayed significantly lower activity, likely due to insufficient nucleation and crystallization of VO_x nanoparticles, which resulted in incomplete heterojunction formation, inefficient charge separation, and reduced generation of reactive oxygen species (ROS) as commonly reported for VO_x/TiO_2 systems [11,16,18].

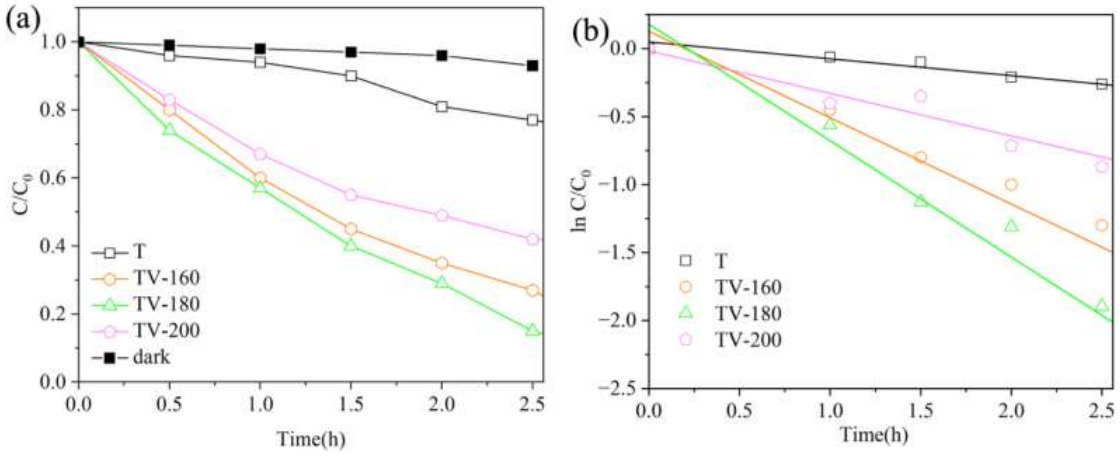

Fig. 2- Photocatalytic activity of T and TV coatings during MB degradation under visible-light exposure: (a) variation of C/C_o with time and (b) plots based on pseudo-first-order kinetics.

On the other hand, treatments at 200 °C led to excessive crystallinity and particle agglomeration, reducing the density of surface-active sites and suppressing heterojunction interfaces, which also diminished photocatalytic performance [19–20]. These observations indicate that 180 °C represents the optimal hydrothermal temperature to balance crystallinity, defect density, and VO_x dispersion for efficient visible-light-driven photocatalysis. Based on this preliminary evaluation, the 180 °C sample was selected as the optimized system for further characterization. To assess its photocatalytic performance, Photocatalytic degradation experiments were conducted under identical conditions as described in Section 2. The suspension was agitated in the absence of light for 30 minutes before irradiation to reach adsorption–desorption equilibrium. The progress of MB degradation was monitored via UV–Vis spectroscopy (Agilent Cary 60), and the photocatalytic degradation efficiency (%) was calculated according to Eq. (1). The photocatalytic degradation of MB can be interpreted using pseudo-first-order kinetics combined with the Langmuir–Hinshelwood model, as represented in Eq. (2) [17,21].

$$ln\left(\frac{C_t}{C_0}\right) = -k_{app}.t \quad (2)$$

The degradation efficiency and degradation kinetics of methylene blue (MB) for the uncoated sample and coated samples prepared at three different temperatures are presented in Figure 3. As observed, the TV-180 sample exhibited the highest photocatalytic performance, achieving a degradation efficiency of approximately 85%, which was superior to all other samples. In addition, the reaction kinetic constant for this sample was higher than those of the other samples, indicating a faster degradation process.

In Figure 4, the diffraction peaks marked with stars can be indexed to anatase TiO_2 (tetragonal structure, JCPDS No. 21-1272). The main reflections observed at $2\theta \approx 25.3°$, 37.8°, and 48.0° correspond to the (101), (004), and (200) planes of anatase TiO_2, respectively. In addition, the peaks marked with triangles are consistent with the presence of orthorhombic V_2O_5 (JCPDS No. 41-1426). Although the VO_x-related peaks are relatively less intense compared to TiO_2, their presence suggests successful hydrothermal deposition of vanadium oxide species on the TiO_2 surface. The crystallite size of the VO_x/TiO_2 composite coating was estimated using the Scherrer equation $D = K\lambda/(\beta \cos \theta)$, where K is the shape factor (taken as 0.9), \lambda is the X-ray wavelength (0.15406 nm for CuKα radiation), \beta is the full width at half maximum (FWHM) of the diffraction peak (in radians), and \theta is the Bragg angle. The FWHM of the anatase (101) reflection was obtained through Gaussian peak fitting. The calculated crystallite size for the optimized TV-180 coating was approximately ~5 nm, indicating the formation of nanocrystalline domains within the composite layer [22].

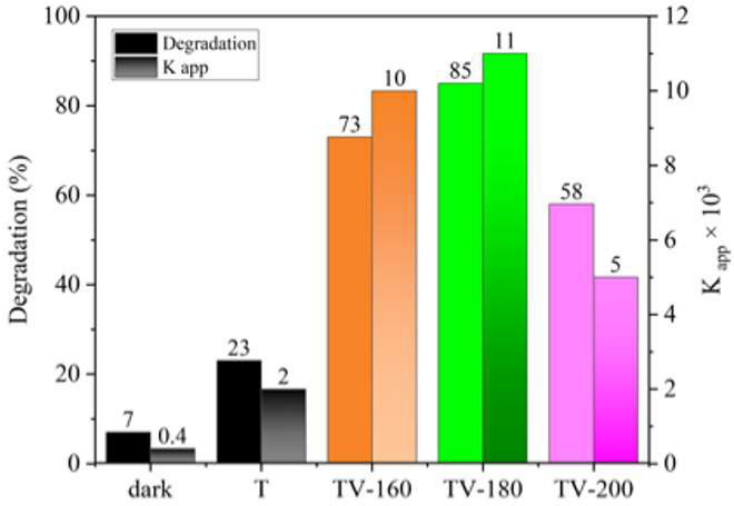

Fig. 3- Evaluation of MB removal efficiencies and calculated rate constants for T and TV-180 coatings at a 6 mM precursor concentration.

Figure 5(a) presents the surface morphology of the bare TiO_2 substrate (T). The sample exhibits a highly porous architecture composed of irregular, interconnected pores with sizes ranging from sub-micron to several microns. This open structure is characteristic of thermally prepared TiO_2 layers and provides a relatively large surface area. In contrast, Figure 5(b) depicts the morphology of the VO_x-coated sample synthesized at the optimized hydrothermal temperature of 180 °C (TV-180). A continuous VO_x overlayer has formed across the surface, partially or completely filling the underlying TiO_2 pores. The surface consists of compact, globular VO_x domains and nanoscale aggregates, consistent with hydrothermal nucleation and growth of vanadium-oxide clusters. This uniform coating suggests the formation of interfacial V–O–Ti species and improved structural cohesion compared to the pristine TiO_2. Compared with the highly porous TiO_2 substrate, the TV-180 sample exhibits fewer open voids, enhanced surface continuity, and a more homogeneous distribution of reactive domains. Such a morphology is advantageous for photocatalysis, as it suppresses surface electron–hole recombination and promotes more efficient charge separation and charge transfer across the TiO_2/VO_x interface [23, 24].

These microstructural characteristics are consistent with the photocatalytic results, in which the TV-180 sample exhibited the highest MB degradation efficiency among the tested temperatures. The optimized hydrothermal coating at 180 °C therefore provides an effective balance between active surface sites and controlled charge-transport pathways, leading to superior visible-light photocatalytic performance.

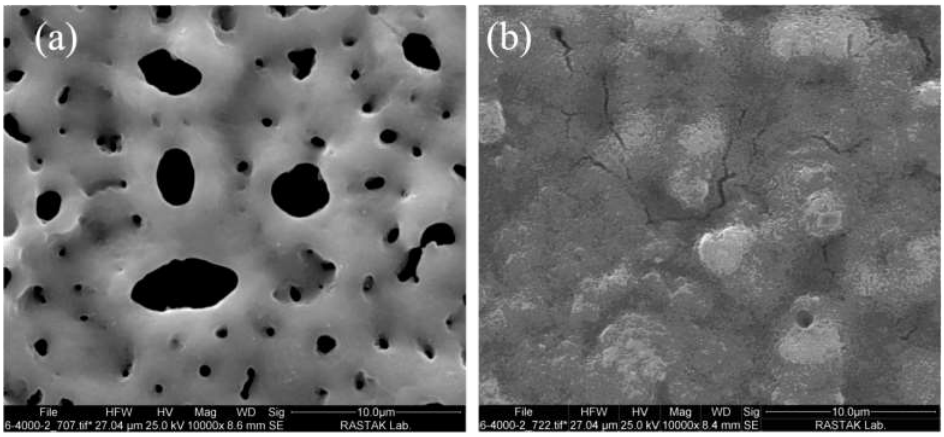

Fig. 4- XRD diffraction pattern of the TV-180 composite coating.

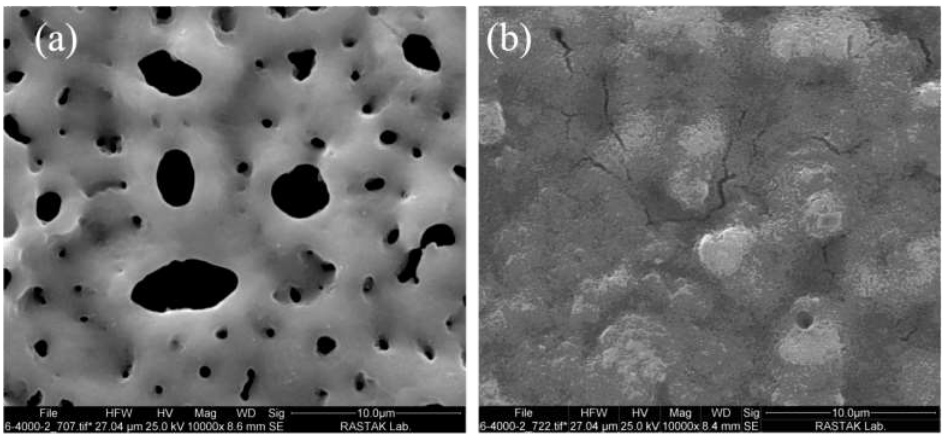

Fig. 5- SEM images showing the surface morphology of coating T (a) and VOx/TiO_2 composites prepared hydrothermally for 24 h (b) with a 6 mM V_2O_5 precursor.

Overall, the photocatalytic performance of the synthesized coatings can be directly correlated with their surface and microstructural characteristics. SEM observations revealed that the optimized TV-180 coating exhibits a more homogeneous VO_x overlayer and improved surface continuity compared to the highly porous pristine TiO_2 coating, thereby favoring efficient interfacial charge transfer. In addition, the enhanced visible-light absorption and red-shifted absorption edge observed in UV–Vis DRS for the VO_x/TiO_2 composite, together with the suppressed PL emission intensity, indicate improved light harvesting and reduced electron–hole recombination. Therefore, the improved MB degradation activity of the TV-180 sample arises from the synergistic combination of favorable surface morphology, nanoscale crystalline domains, and improved charge separation at the VO_x/TiO_2 interface.

In addition to hydrothermal temperature, several key parameters can influence the final properties and photocatalytic performance of VO_x/TiO_2 coatings. The vanadium precursor concentration governs the VO_x loading and dispersion on the TiO_2 surface; excessively high concentrations may lead to particle agglomeration and blockage of active sites, while insufficient loading may limit heterojunction formation [5,20]. The hydrothermal reaction time affects crystal growth and phase evolution, where prolonged durations can enhance crystallinity but may also promote grain coarsening [17]. Furthermore, the pH of the precursor solution plays a crucial role in controlling the speciation of vanadium complexes and their deposition behavior [16]. In addition, intrinsic features of the PEO layer, such as pore size, surface roughness, and oxide thickness, significantly influence the nucleation and anchoring of VO_x species [13,15]. These factors collectively determine the balance between surface area, crystallinity, and interfacial charge-transfer efficiency, ultimately governing the photocatalytic performance of the composite system.

According to the Tauc plot shown in Figure 6 a, the optimal sample exhibits a band gap of approximately 1.75 eV, which is significantly lower than that of TiO_2 (≈3.2 eV). This band-gap narrowing enhances visible-light absorption and consequently improves the photocatalytic activity of the composite coating, also in Figure 6 b. The red-shift of the absorption edge from 402 to 602 nm indicates a substantial band-gap narrowing, which enhances visible-light harvesting and contributes to the improved photocatalytic performance of the VO_x-modified TiO_2 coating. The optical band gap values were evaluated based on Tauc's relation (Eq. 3) [25]:

$$(\alpha hv) = B((\alpha hv) - E_g)^n \quad (3)$$

In this relation, h denotes Planck's constant, ν corresponds to photon frequency, α is the absorption coefficient, B represents a proportionality constant, and Eg indicates the band gap energy. The exponent n is determined by the type of electronic transition, with n = 0.5 applied for direct transitions and n = 2 for indirect ones [26]. Experimentally, the band gap was obtained by extrapolating the linear segment of the versus hv curve to its intersection with the hv axis, as illustrated in Figure 6b [25].

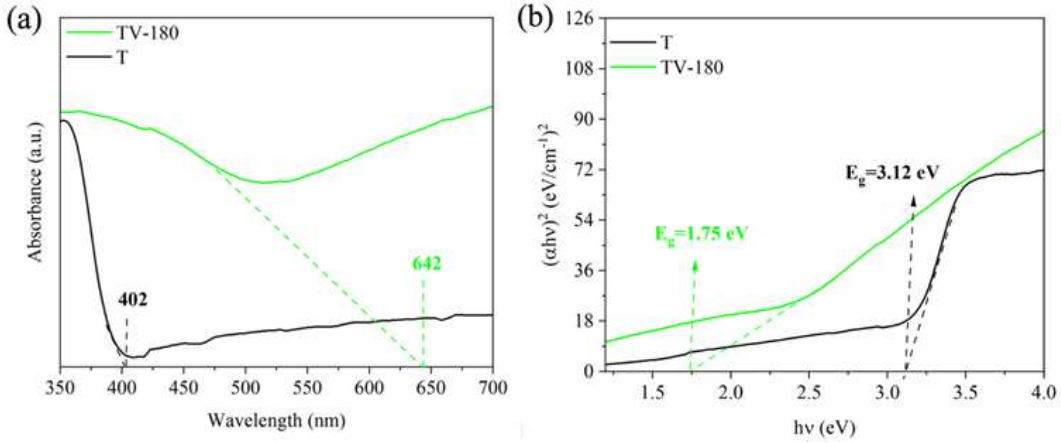

Fig. 6- (a) Absorbance spectra of T and TV-180 coatings, and (b) their Tauc plots used for band-gap evaluation.

The PL spectrum of the TiO_2 substrate coated with a hydrothermally grown VO_x layer (Figure 7) consists of three distinct components. The high-energy component at ≈3.15 eV corresponds to the band-edge recombination of anatase TiO_2, whereas the mid-energy peak at ≈2.65 eV is attributed to defect-related recombination associated with oxygen vacancies and Ti^{3+} centers. The low-energy component (≈2.05 eV) is consistent with intermediate states and transitions related to the vanadium-oxide layer (V^{4+}/V^{5+}) or with interfacial charge-transfer processes between VO_x and TiO_2. The strong defect-related emission accompanied by the relative suppression of the band-edge peak indicates electron trapping in mid-gap states and effective charge separation at the TiO_2/VO_x interface, which may account for the enhanced photocatalytic activity of the sample under visible-light irradiation [27–29].

To gain further insight into the photocatalytic mechanism, qualitative radical scavenger analysis was performed using isopropanol (IPA), sodium azide (NaN_3), and benzoquinone (BQ), which are known to quench •OH, (•OH + $^1O_2$), and $O_2•^-$ species, respectively. The results indicated that the presence of IPA and NaN_3 noticeably suppressed the degradation efficiency, suggesting that hydroxyl radicals (•OH) play a dominant role in the photocatalytic process. The additional inhibitory effect observed with NaN_3 also implies the contribution of singlet oxygen ($^1O_2$). In contrast, the effect of BQ was comparatively less pronounced, indicating that superoxide radicals ($O_2•^-$) participate in the reaction but are not the primary active species. Based on these observations, the reactive species involved in MB degradation can be qualitatively ranked as:

$$•OH > {}^1O_2 \approx O_2•^-$$

These findings suggest that the VO_x/TiO_2 heterostructure facilitates efficient charge separation under visible-light irradiation, leading to the generation of reactive oxygen species. Photogenerated holes contribute to the formation of •OH, while electrons reduce dissolved oxygen to form $O_2•^-$, which may further participate in secondary ROS generation [4,19,30]. The scavenging results are consistent with previous studies on TiO_2-based and VO_x-modified photocatalysts, where •OH radicals are identified as the dominant reactive species, while $O_2•^-$ and $^1O_2$ act as secondary contributors [28, 30]. Furthermore, VO_x incorporation has been reported to enhance charge separation and promote ROS generation through the formation of interfacial electronic states [19]. The generation of •OH via hole oxidation and $O_2•^-$ via electron transfer to dissolved oxygen has been extensively reported in TiO_2-based heterostructures [5]. The Schematic illustration of the proposed photocatalytic mechanism over VO_x/TiO_2 (TV-180) under visible light is represented in Figure 8.

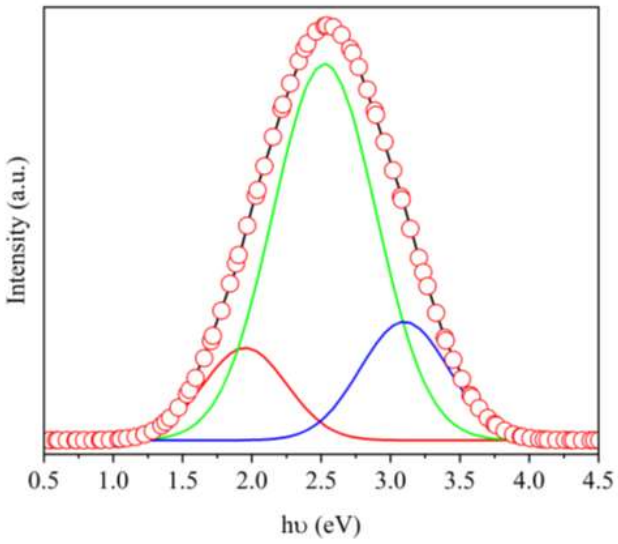

Fig. 7- PL emission spectra and peak deconvolution of the TV-180 coating.

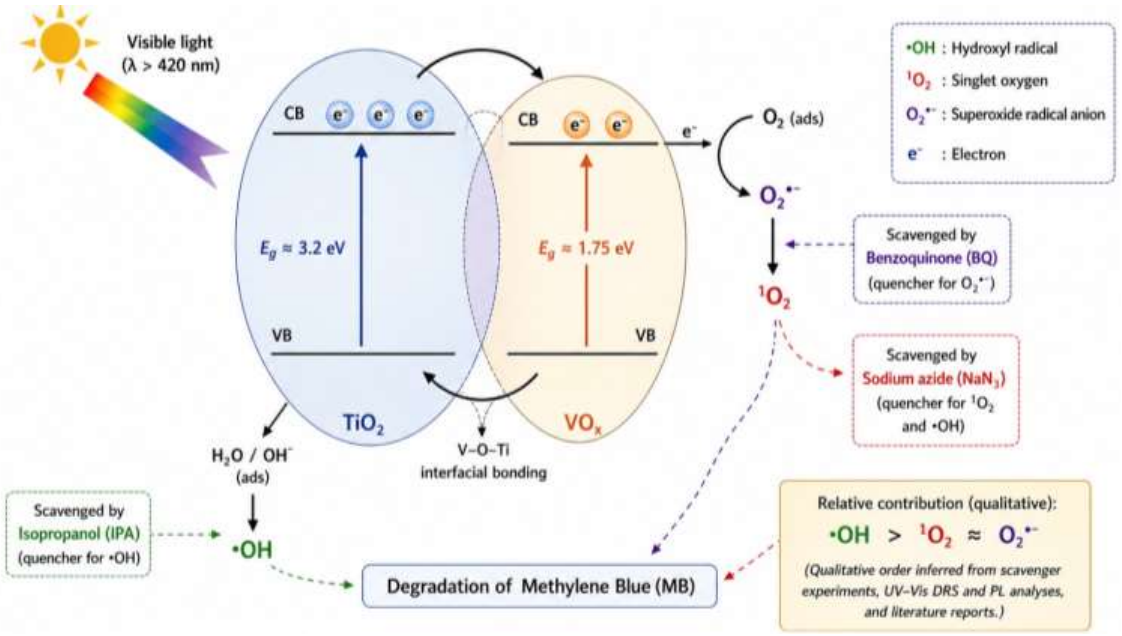

Fig. 8- Schematic illustration of the proposed photocatalytic mechanism over VO_x/TiO_2 (TV-180) under visible light, highlighting charge separation and the generation of reactive oxygen species (•OH, O_2•$^-$, and $^1O_2$) involved in MB degradation. The exact charge transfer pathway remains inconclusive.

4. Conclusions

Optical studies demonstrated an apparent optical band gap (~1.75 eV) and a red-shifted absorption edge, associated with VO_x-induced electronic states and interfacial charge-transfer transitions. This apparent reduction in transition energy is attributed to the formation of VO_x-related mid-gap states and V–O–Ti interfacial bonding, which introduce additional sub-band-gap absorption pathways under visible-light irradiation. Importantly, this value does not indicate a fundamental narrowing of the intrinsic TiO_2 band gap (~3.2 eV), but rather reflects composite-induced electronic interactions that enhance visible-light harvesting and photocatalytic efficiency. Photoluminescence measurements indicated effective charge separation at the TiO_2/VO_x interface. Overall, the optimized VO_x/TiO_2 composite exhibits superior visible-light-driven photocatalytic performance, underscoring the effectiveness of the PEO–hydrothermal strategy for environmental remediation applications.

References

1. S. Sakthivel, M.C. Hidalgo, D.W. Bahnemann, S.-U. Geissen, V. Murugesan, A. Vogelpohl, A Fine Route to Tune the Photocatalytic Activity of TiO2, Appl. Catal. B 63 (2006) 31–40.
2. J. Jeon, D.H. Kweon, B.J. Jang, M.J. Ju, J. Baek, Enhancing the Photocatalytic Activity of TiO2 Catalysts, Adv. Sustain. Syst. 4 (2020).
3. J.C. Crittenden, J. Liu, D.W. Hand, D.L. Perram, Photocatalytic Oxidation of Chlorinated Hydrocarbons in Water, Water Res. 31 (1997) 429–438.
4. F. Ren, H. Li, Y. Wang, J. Yang, Enhanced Photocatalytic Oxidation of Propylene over V-Doped TiO2 Photocatalyst, Appl. Catal. B 176–177 (2015) 160–172.
5. X. Zhou, J. Wu, Q. Li, Y. Qi, Z. Ji, P. He, X. Qi, P. Sheng, Q. Li, J. Ren, Improved Electron–Hole Separation and Migration in V2O5/Rutile–Anatase Photocatalyst System,Chem. Eng. J. 330 (2017) 294–308.
6. J. Sun, X. Li, Q. Zhao, J. Ke, D. Zhang, Novel V2O5/BiVO4/TiO2 Nanocomposites with High Visible-Light Photocatalytic Activity, J. Phys. Chem. C 118 (2014) 10113–10121.
7. M. Ghosh, J. Liu, S.S.C. Chuang, S.C. Jana, Hierarchical V2O5 Nanorods on TiO2 Nanofibers, ChemCatChem 10 (2018) 3305–3318.
8. Y. Wang, Y.R. Su, L. Qiao, L.X. Liu, Q. Su, C.Q. Zhu, X.Q. Liu, One-Dimensional TiO2/V2O5 Heterostructures, Nanotechnology 22 (2011) 225702.
9. Q. Su, J. Zhang, Y. Wang, M. Yu, C. Zhu, W. Lan, X. Liu,Effect of Morphology on V2O5/TiO2 Photocatalysts, J. Phys. Chem. Solids 74 (2013) 1475–1481.

10. M. Motola, L. Satrapinskyy, M. Čaplovicová, T. Roch, M. Gregor, Enhanced Photocatalytic Activity of V-Doped TiO2 Nanotubes, Appl. Surf. Sci. 434 (2018) 1257–1265.
11. T. Karras, M. Aittala, T. Aila, S. Laine, Alias-Free Generative Adversarial Networks, arXiv preprint arXiv:2205.04046 [cs. CV] (2022).
12. V.T. Truong, P.N.M. Le, M.V. Le, Influence of Hydrothermal Parameters on Photocatalytic Activity of BiVO4 for Degradation of Methylene Blue, Indonesian Journal of Chemistry 25 (2025) 744–759.
13. A.L. Yerokhin, X. Nie, A. Leyland, A. Matthews, S.J. Dowey, Plasma Electrolysis for Surface Engineering, Surf. Coat. Technol. 122 (1999) 73–93.
14. A.L. Yerokhin, A. Matthews, Plasma Electrolytic Oxidation of Aluminium Alloys, Thin Solid Films 515 (2007) 147–158.
15. M. Kaseem, Y.G. Ko, Recent Advances in Plasma Electrolytic Oxidation, Coatings 9 (2019) 283.
16. J. Livage, Hydrothermal Synthesis of Vanadium Oxides, Materials 3 (2010) 4175–4195.
17. M. Tang, Y. Xia, D. Yang, et al., Hydrothermal Parameters on TiO2 Structure, Materials 14 (2021) 5674.
18. A. Saberyoun, A. Fattah-alhosseini, M. Karbasi, R. Hosseini, M. Kaseem, Visible-Light Photocatalytic Cu/TiO2 Coatings, Ceram. Int. 50 (2024) 31313–31325.
19. H. Zhang, D. Meng, B. Fu, H. Fan, R. Cai, P.P. Fu, X. Wu, Separation of charge carriers and generation of reactive oxygen species by TiO 2 nanoparticles mixed with differently-coated gold nanorods under light irradiation, Journal of Environmental Science and Health, Part C 37 (2019) 81–98.
20. A. Nellessen, A. Schaefer, A. Martinelli, et al., Vanadium Loading on Titania, J. Phys. Chem. C 128 (2024) 2894–2908.
21. J. Vujančević, P. Andričević, V. Djokić, et al.,Vanadium-Oxide Modified TiO2, Catalysts 13 (2023) 352.
22. G.-W. Lin, J.-S. Chen, W. Tseng, F.-H. Lu, Anatase TiO2 Coatings by PEO, Surf. Coat. Technol. 357 (2019) 28–35.
23. A.L. Patterson, The Scherrer Formula for X-Ray Particle Size Determination, Phys. Rev. 56 (1939) 978–982.
24. A. Hoseini, B. Yarmand, Fe2O3/TiO2 via PEO, J. Nanopart. Res. 22 (2020) 312.
25. M. Laghaei, M. Ghasemian, M.R.G. Ferdowsi, et al., Titanium–Vanadium Oxides, J. Colloid Interface Sci. 646 (2023) 11–24.
26. K. Schneider, Electronic Structure of Vanadium Oxides, J. Mater. Sci.: Mater. Electron. 31 (2020) 10478–10488.
27. C. Huang, L. Chen, H. Li, et al., Bi2WO6 Photocatalysis, RSC Adv. 9 (2019) 27768–27779.
28. S. Lettieri, M. Pavone, A. Fioravanti, et al., Charge Carrier Processes in TiO2, Materials 14 (2021) 1645.
29. L. Kernazhitsky, V. Shymanovska, T. Gavrilko, et al., Photoluminescence of TiO2, J. Lumin. 166 (2015) 253–258.
30. Y. Wang, Q. Su, C.H. Chen, et al., V2O5 Nanomaterials Growth, J. Phys. D: Appl. Phys. 43 (2010) 185102.